That can be integrated, so

$$m_1(t_{-1}, t_0, x) = m_0(x) \int_0^{t_{-1}} D_0(t'_{-1}) dt'_{-1} + f(0, t_0, x) \tag{4.2.13}$$

In this context, we chose not to label the integration constant as $u_1(t_{-1} = 0)$ because the assumption we made about m_0 holds asymptotically, rather than from $t = 0$. There might be a transient regime influenced by the initial condition $m(x, t = 0)$, which we are not interested in analyzing here. Consequently, we can express

$$m_1(t_{-1}, t_0, x) = m_0(x) \int_{\tau_{-1}(t_0,x)}^{t_{-1}} D_0(t'_{-1})\, dt'_{-1}$$

This equation provides a formula to find the first-order correction m_1. However, since we do not have additional equations to determine the function $\tau_{-1}(t_0, x)$, we are unable to calculate the first-order correction to the kink's shape m_1 in this limit of rapidly-oscillating $C(t)$.
The position of the kink is not affected by $C(t)$. We decided to not prove this statement here, but in the next section, while studying the fast oscillations limit in a 2D system. Then a 1D system can be recovered from a 2D one by taking the limit where the curvature of any interface $\kappa \to 0$.

4.3 The 2D case

In the previous chapter, we showed that it is not possible to control the position of a kink in a 1D system using a time-dependent control parameter $C(t)$. Precisely, this conclusion was reached by examining two limiting cases: first, when the oscillations of $C(t)$ are slow relative to the system's intrinsic timescale τ_{linear} and $C(t)$ remains strictly positive, and second, when the oscillations are fast compared to τ_{linear}, requiring just the average value of $C(t)$ being positive.
In this chapter, we will demonstrate that a similar result holds for 2D systems: the *motion by curvature*, which governs the dynamics of interfaces, remains unaffected by the modulation of $C(t)$ in these limiting cases, at least to leading order.
The key difference between the 1D and 2D analysis of dynamics is the introduction of curvature in 2D. This introduces a new timescale, linked to the time required for an interface to move over a distance comparable to its thickness. We will examine the scenario where $C(t)$ varies slowly over time, such that the timescale of $C(t)$'s variation aligns with the new timescale introduced by curvature. This curvature timescale is shorter than the system's intrinsic timescale, $\tau_{\text{linear}} \sim \frac{1}{C}$. We will also examine the case where $C(t)$ varies rapidly compared to the intrinsic timescale τ_{linear}. In both scenarios, we will find that, to leading order, the motion by curvature is not influenced by the time-dependent $C(t)$.

4.3.1 Slow varying temperature

In Sec. 2.3, we noted that during the asymptotic dynamics, the curvature κ at any point on the interface is small, and the interface propagates slowly without

changing its shape to leading order. By combining these observations with the scaling hypothesis, we derived the following equations:

$$\kappa = \epsilon K_1; \quad K_1 \sim 1, \tag{4.3.1}$$

$$\Delta = \partial_{\xi\xi} + \epsilon K_1 \partial_\xi + O(\epsilon^2); \quad \epsilon \ll 1, \tag{4.3.2}$$

$$\partial_t m = -\epsilon V_1 \partial_\xi m; \quad V_1 \sim 1. \tag{4.3.3}$$

In Sec. 2.3, the control parameter C was held constant. However, in the present analysis, we consider a time-dependent $C(t)$, given by:

$$C(t) = \bar{C} + D_0(t),$$

where $D_0(t)$ is a periodic oscillation with $D_0(t+T) = D_0(t)$, and $\bar{C}$ is the average value around which $C(t)$ oscillates.
We define $C(t)$ as slowly varying if its variation occurs at a timescale that is slow compared to the intrinsic timescale of the dynamics, $\tau_{\text{linear}} \sim \frac{1}{\bar{C}} \sim 1$ (assuming $\bar{C} \sim 1$). Specifically, $C(t)$ is considered slowly varying if its timescale is comparable to the timescale of the interface propagation, a phenomena described by Eq. 4.3.3. Introducing the new time variables:

$$t_0 = t; \quad \tau = \epsilon t,$$

the slow varying limit, similar to the 1D analysis, corresponds to:

$$C(t) = \tilde{C}(\tau) \implies \partial_t C = \epsilon \partial_\tau C,$$

where the small parameter ϵ appearing in the last equation is the same as that in Eq. 4.3.3. In general, the introduction of t_0 and τ leads to the relation:

$$\partial_t = \partial_{t_0} + \epsilon \partial_\tau.$$

However, to incorporate in the last expression the phenomena of interface propagation described in Eq. 4.3.3, we state:

$$\partial_t = \partial_{t_0} + \epsilon \partial_\tau - \epsilon V_1 \partial_\xi. \tag{4.3.4}$$

And using the properties 4.3.1, 4.3.2 and 4.3.4 in the TDGL equation

$$\partial_t m = \Delta m + C(t) m - m^3$$

we find, up to leading order in ϵ

$$\partial_{t_0} m + \epsilon \partial_\tau m = \partial_{\xi\xi} m + \epsilon (K_1 + V_1) \partial_\xi m + \tilde{C}(\tau) m - m^3 \tag{4.3.5}$$

As we did during the 1D analysis, we expand the order parameter in powers of ϵ

$$m = m_0 + \epsilon m_1 + O(\epsilon^2)$$

and by putting this expansion in the TDGL equation (Eq. 4.3.5) and equating the terms of order zero (ϵ^0), we find

$$\partial_{t_0} m_0 = \partial_{\xi\xi} m_0 + \tilde{C}(\tau) m_0 - m_0^3 \tag{4.3.6}$$

To order zero, we find the same equation we found in the 1D analysis, where $x \to \xi$. In that previous analysis, we found

$$m_0(\xi, t) = \sqrt{C(\tau)} \tanh\left(\xi \sqrt{\frac{\tilde{C}(\tau)}{2}}\right)$$

Before equating the terms of order ϵ^1 in Eq. 4.3.5, we apply the same assumptions as in the 1D analysis:

$$m_i(\xi, t) = \beta_i(t) m_{k_i}(\alpha_i(t)\xi),$$
$$\alpha_1 = \alpha_0 \equiv \alpha,$$
$$\partial_{t_0}\alpha = \partial_{t_0}\beta_1 = 0.$$

Under these assumptions, equating the terms of order ϵ^1 in the TDGL equation yields:

$$\alpha^2\beta_1\left(m''_{k_1} + m_{k_1} - 3m_{k_0}^2 m_{k_1}\right) = \alpha'\left(m_{k_0} + u'_{k_0}\chi\right) - (K_1 + V_1)\alpha^2 m'_{k_0}. \tag{4.3.7}$$

Here, $\chi \equiv \alpha\xi$, $\alpha' \equiv \partial_\tau \alpha$, and $m'_{k_i} \equiv \partial_\chi m_{k_i}$.
Note that this is the same equation found in the 1D analysis (Eq. 4.2.5), but with an additional term $(K_1)\alpha^2 m'_{k_0}$. The term containing V_1 was also absent in the 1D analysis, though not for any physical reason. Rather, we decided to take into account the influence of $C(t)$ on the kink's position directly in the current analysis of a 2D system, whereas this was not accounted for in the previous 1D study.
The presence of additional terms in the equation neglects the possibility of retrieving an equation with only spatial derivatives, as was done in the 1D analysis. That's because, if we follow the same approach and require:

$$\alpha^2\beta_1 = \alpha' = \alpha^2,$$

considering that $\alpha = \sqrt{\tilde{C}(\tau)}$, we obtain a constraint on $\tilde{C}(\tau)$ that does not align with the requirement for $C(t)$ to be a periodic function.
However, we can still extract useful information from Eq. 4.3.7 by applying the Fredholm alternative, a theorem discussed in Sec. 2.3. As we're dealing with a differential equation of this kind

$$\hat{L}u(\chi) = f(\chi),$$

where

$$\hat{L} = \partial_{\chi\chi} + (1 - 3u_{k_0}^2)$$

It follows that, if $v(\chi)$ is an homogeneous solution ($\hat{L}v = 0$), then

$$\int_{-\infty}^{+\infty} f(\chi)v(\chi)\,d\chi = [\partial_\chi uv - u\partial_\chi v]_{-\infty}^{+\infty}. \tag{4.3.8}$$

In our case, a solution of the homogeneous equation is gived by $u_{k_1} = \partial_\chi u_{k_0}$, as this follows from differentiating Eq. 4.3.6. While

$$f(\chi) = \alpha'(u_{k_0} + \partial_\chi u_{k_0}\chi) - \alpha^2(K_1 + V_1)\partial_\chi u_{k_0}.$$

Assuming the boundary terms are zero, we apply the Fredholm alternative:

$$\int f(\chi)\partial_\chi u_{k_0}(\chi)\,d\chi = 0.$$

$$\int \alpha'(u_{k_0}\partial_\chi u_{k_0} + (\partial_\chi u_{k_0})^2\chi)d\chi - \int \alpha^2(K_1 + V_1)(\partial_\chi u_{k_0})^2 d\chi = 0$$

And recognizing the properties:

- u_{k_0} is odd, so $\partial_\chi u_{k_0}$ is even;
- $(\partial_\chi u_{k_0})^2$ is always positive (or its integral is strictly positive);
- The integration domain is symmetric.

We conclude that:

$$V_1 = -K_1.$$

This implies that, up to leading order, the motion by curvature is unaffected by a time-dependent control parameter $C(t)$. Notably, by utilizing the identity $V_1 = -K_1$ in Eq. 4.3.7, we recover the corresponding equation found in the 1D analysis (Eq. 4.2.5). Thus, we can conclude, without requiring further calculations, that up to leading order, the shape of an interface along a direction perpendicular to it is the same as that of a 1D kink.

Numerical evidence

We numerically verified the motion by curvature equation $v = -\kappa$ by examining an isolated circular domain, whose radius $R(t)$ decreases over time. This example is detailed in Sec. 2.3, where the preparation of the initial state and the method for measuring the radius $R(t)$ over time are explained.
In Sec. 2.3, the control parameter C was constant over time, whereas in this section, $C(t)$ is time-dependent. Specifically, we used the form:

$$C(t) = \bar{C} + A\sin\left(2\pi\frac{t}{T}\right),$$

with the requirement that $C(t)$ be slowly varying over time, which translates to $T \sim \epsilon^{-1}$. This small parameter ϵ also describes the smallness of the curvature $\kappa \sim \epsilon$, given that $\kappa = \frac{1}{R}$ for a circular domain. Consequently, we prepared the initial state by selecting

$$T = R_0,$$

where R_0 is the initial radius of the isolated circular domain.

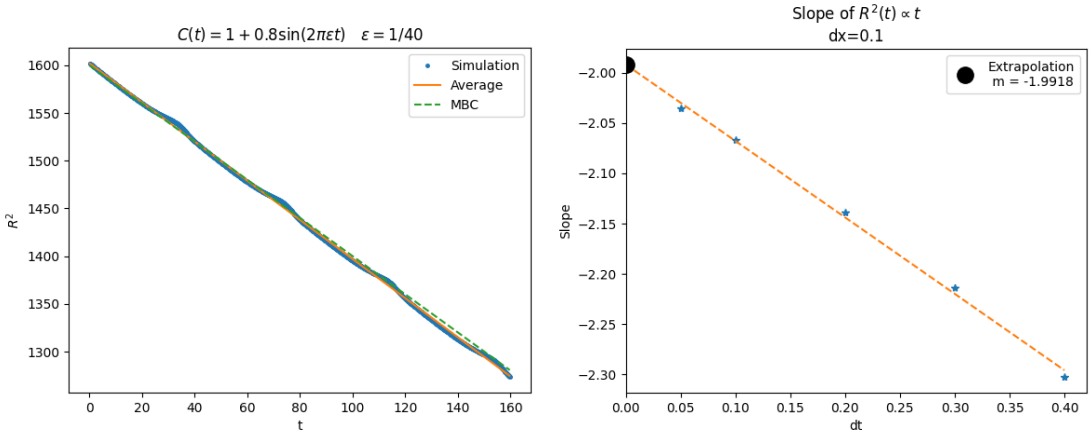

Figure 4.3: On the **left**: Square of the radius of an isolated circular domain $R(t)^2$ as a function of time, where $C(t) = 1 + 0.8\sin(2\pi\epsilon t)$ and $\epsilon = R(0)^{-1} = 1/40$. The blue curve correspond to the measured value of $R(t)^2$. The orange line is a time average, computed making a linear fit of the blue curve. While the green line corresponds to the expected relation if motion by curvature ($v = -\kappa$) holds: $R(t)^2 = R_0^2 - 2t$. The simulation parameters are $dt = 0.1$, $dx = 0.1$, $L = 128$, $R(0) = 40$. On the **right**: The simulation on the left was carried for multiple values of dt. Each time the slope of the experimental curve (the blue one) was estimated with a linear fit. Here the estimated slope is represented as a function of dt. A linear regression to extrapolate the slope value at $dt \to 0$ returns the value -1.992 ± 0.006, that is compatible with the expected value (-2) within two standard deviations.

In Figure 4.3 (left), the measured value of $R^2(t)$ during the simulation is plotted as a function of time. If motion by curvature is valid, we expect $R^2(t)$ to decay linearly, as demonstrated in Sec. 2.3:

$$R^2(t) = R_0^2 - 2t.$$

This linear decay is observed, particularly when the measures of $R^2(t)$ (shown by the blue curve) are averaged over time (orange line). However, the decay appears to be slightly faster than expected (green line).
This discrepancy can be attributed to the discreteness of time steps used in the simulations. To address this, Figure 4.3 (right) illustrates the estimation of the slope of the orange curve by running simulations with various time step values dt. An extrapolation to $dt \to 0$ confirms the expected value of the slope, thereby validating the motion by curvature behavior in the simulations.

4.3.2 Fast varying temperature

This scenario represents the opposite limit, where the time scale associated with the variations of $C(t)$ is one order of magnitude larger than the intrinsic time scale